Report No. ACNP-63016

PATHFINDER ATOMIC POWER PLANT TECHNICAL PROGRESS REPORT

JANUARY 1963 - MARCH 1963

Submitted to

U. S. ATOMIC ENERGY COMMISSION
NORTHERN STATES POWER COMPANY
and
CENTRAL UTILITIES ATOMIC POWER ASSOCIATES

by

ALLIS-CHALMERS MANUFACTURING COMPANY
ATOMIC ENERGY DIVISION
Milwaukee 1, Wisconsin

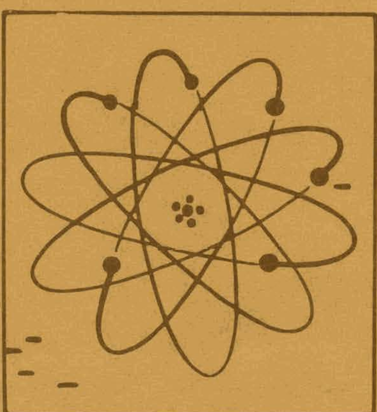

Facsimile Price $ 4.60
Microfilm Price $ 1.58

Available from the
Office of Technical Services
Department of Commerce
Washington 25, D. C.

Ref: AEC Contract No. AT(11-1)-589

DISCLAIMER

LEGAL NOTICE

ACNP-63016

PATHFINDER ATOMIC POWER PLANT
TECHNICAL PROGRESS REPORT

JANUARY 1963 – MARCH 1963

Submitted to

U. S. ATOMIC ENERGY COMMISSION
NORTHERN STATES POWER COMPANY
and
CENTRAL UTILITIES ATOMIC POWER ASSOCIATES

by

ALLIS-CHALMERS MANUFACTURING COMPANY

Under
Agreement dated 2nd Day of May 1957, as Amended
between
Allis-Chalmers Mfg. Co. & Northern States Power Co.
under
AEC Contract No. AT(11-1)-589

June 15, 1963

Classification – UNCLASSIFIED

Reviewed by RW Klecker
Authorized Classifying Official

Approved: C. B. Graham
C. B. Graham
Manager
Nuclear Power Dept.-Greendale

Approved: Hibbert Hill
Hibbert Hill
Vice President-Engineering

ALLIS-CHALMERS MANUFACTURING COMPANY
ATOMIC ENERGY DIVISION
MILWAUKEE 1, WISCONSIN

NORTHERN STATES POWER COMPANY
15 SOUTH FIFTH STREET
MINNEAPOLIS 2, MINNESOTA

ACNP-63016

PATHFINDER ATOMIC POWER PLANT

TECHNICAL PROGRESS REPORT

JANUARY 1963 - MARCH 1963

DISTRIBUTION

USAEC, Chicago Operations Office-- 9800 South Cass Avenue, Argonne, Illinois	5
USAEC, Division of Reactor Development-- Washington 25, D.C.	8
USAEC, OTIE-- Oak Ridge, Tennessee ... OFFSET MASTER PLUS	20
Northern States Power Company and CUAPA	26
Allis-Chalmers Manufacturing Company	39
Total	98

CONTENTS

ILLUSTRATIONS

Figure Number	Title	Page

POST CONSTRUCTION

FOREWORD

This is one of a series of reports covering technical progress on the research and development program being performed in connection with the design of the Pathfinder Atomic Power Plant. This plant will be located at a site near Sioux Falls, South Dakota and is scheduled for operation in 1963. Owners and operators of the plant will be the Northern States Power Company of Minneapolis, Minnesota.

The U. S. Atomic Energy Commission, through Contract No. AT(11-1)-589 with Northern States Power Company, and Central Utilities Atomic Power Associates* (CUAPA), are sponsors of the research and development program.

Allis-Chalmers Manufacturing Company of Milwaukee, Wisconsin, under contract with Northern States Power Company, is performing the research, development, and design; and will construct the plant including the reactor, which is designated the Controlled Recirculation Boiling Reactor (CRBR) with Nuclear Superheater. Pioneer Service and Engineering Company of Chicago, Illinois is providing the architect-engineer services to Allis-Chalmers. Portions of the R & D program, particularly in connection with fuel development, have been subcontracted by Allis-Chalmers.

---

*CUAPA MEMBER COMPANIES:

Interstate Power Company
Iowa Power and Light Company
Iowa Southern Utilities Company
Madison Gas and Electric Company
Northern States Power Company
Northwestern Public Service Co.
Otter-Tail Power Company
St. Joseph Light & Power Co.
Western Power and Gas Company
Wisconsin Public Service Corp.

DESIGN DATA

CRBR WITH NUCLEAR SUPERHEATER

Plant

Power, boiler region	157,200 kw
Power, superheater region	42,400 kw
Steam flow at rated power	616,125 lbs/hr
Total core power	199,600 kw
Gross electrical capability	66,000 kw
Net electrical output	62,000 kw
Net efficiency	31.0 per cent
Steam outlet pressure (reactor)	535 psig
Reactor operating pressure	600 psig
Temperature, boiler region	489 F
Outlet temperature, superheater region	825 F
Gross heat rate	10,199 Btu/kw-hr
Reactor building size	50 ft dia x 120 ft

Reactor

Vessel size (over-all)	11 ft 6 in o.d. 36 ft 1 in
Total core dimensions	6 ft x 6 ft
Dimensions of superheater region	6 ft x 30 in
Fuel, boiler (Zr-2 clad)	approx. 2.2 per cent enriched UO_2
Fuel, superheater (S.S. clad)	approx. 93 per cent enriched UO_2
Fuel, loading, boiler (U-235)	145.6 kg
Fuel, loading, superheater (U-235)	42 kg
Power density (boiler core coolant)	87 kw/liter
Average heat flux, boiler region	128,000 Btu/hr-ft^2
Average heat flux, superheater region	77,800 Btu/hr-ft^2
Maximum heat flux, boiler region	462,000 Btu/hr-ft^2
Maximum heat flux, superheater region	245,000 Btu/hr-ft^2
Recirculation rate	65,000 gpm
Recirculation pump power	823 kw
Neutron flux	approx. 5×10^{13} n/cm^2sec

I. FUEL ELEMENT RESEARCH AND DEVELOPMENT

1.1 FUEL MATERIAL CLADDING, BONDING, AND IRRADIATION TESTING

The objectives of this project are as follows: 1) to perform laboratory work on the material and thermal properties of boiler fuel elements in the following two general areas: (a) fuel cladding testing and investigations as required, and (b) complete aluminum capsule irradiation proof-testing together with pre- and post-irradiation examinations; 2) to develop a high-enrichment uranium dioxide stainless steel cermet fuel element clad with stainless steel or a suitable alternate material, which includes development of means of maintaining alignment and spacing of fuel bearing tubes and double-walled insulating tubes, development of conceptual designs for the steam entry and exit section supporting the element, evaluation of assembly techniques, and fabrication of a steam corrosion-erosion test loop and testing of superheater fuel cladding material; and 3) to develop means of inserting burnable poison in the reactor core, as required, and to perform studies and research and development on in-core instrumentation for the boiler region flux and coolant flow distribution and for superheater region temperature, flux and coolant flow.

1.1.1 STEAM CORROSION-EROSION TEST ON STAINLESS STEELS

Only limited information is presently available on corrosion-erosion characteristics of various stainless steels in oxygenated steam and superheated steam. Conventional plants use stainless steel in some superheater sections but the exposure is to essentially oxygen-free steam. Nuclear superheater fuel cladding, however, will be exposed to conditions ranging from saturated to superheated steam containing oxygen.

The tests described here had the objectives of determining corrosion-erosion characteristics of stainless steel in dynamic saturated oxygen containing steam...determining corrosion-erosion as a function of moisture content of the steam...and determining corrosion-erosion in dynamic superheated steam.

Test Procedure

Figure 1.1 shows the general layout of the test apparatus and Figure 1.2 shows the appearance of the operating loop. The loop functions have been previously described in ACNP-6123, Pathfinder Technical Progress Report, July-September, 1961. To briefly review these functions:

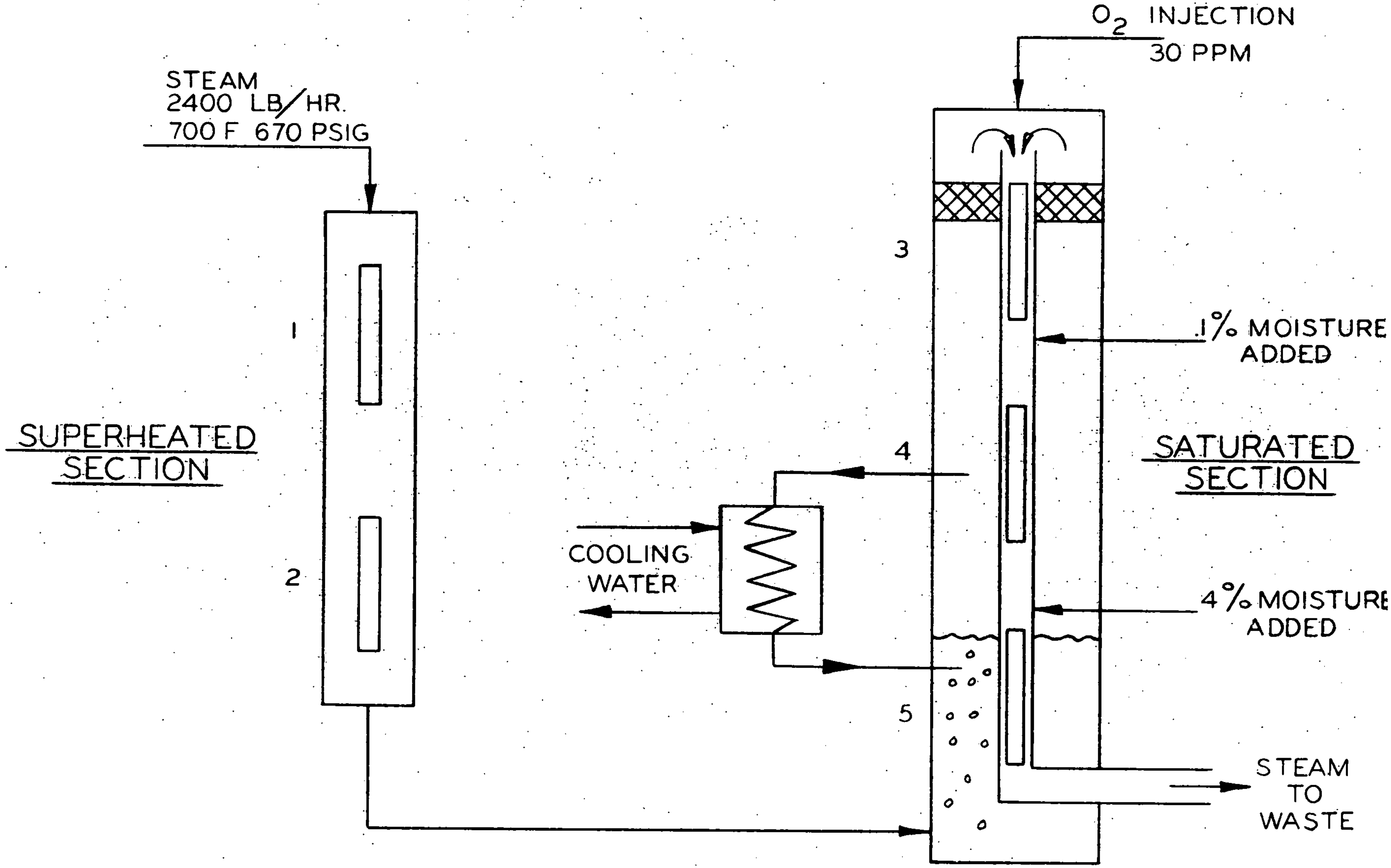

Fig. 1.1...Schematic Flow Diagram of Corrosion-Erosion Facility (43-024-971)

Fig. 1.2...Corrosion-Erosion Loop (212195)

Superheated steam was passed over a cluster of specimens... through a "reboiler" to give saturated conditions...dried by passage through a demister...followed by the injection of oxygen. The oxygenated, saturated steam was then passed over three sets of specimens. Moisture was injected into the steam between the stations to give 0.1 and 0.5 per cent moisture respectively in the steam passing over the last two sections. Chloride was maintained at an average concentration of 0.15 ppm in the "reboiler" by periodic blowdown.

Table 1.1 indicates the test conditions which existed at the various test stations for the 2500-hour test period.

Table 1.1

	Superheated Steam Station	Saturated Steam Stations A	B	C
Flow (fps)	250	175	175	175
Pressure (psi)	670	600	600	600
Temperature ($^{\circ}$F)	700	489	489	489
Moisture (%)	---	0.0	0.1	0.5
Oxygen (ppm)	---	30	30	30

At the start of testing, all stations were loaded with 304L and 316L stainless steel. At 500-hour intervals a specimen of each type was removed from each station and replaced with a Type 304 and 316 stainless steel specimen respectively. The specimens consisted of two-inch lengths cut from fully annealed tubing of the composition given in Table 1.2. It should be noted that the 316 SS used for this test actually had an analysis within the 316L SS range of composition. As may be expected from the similarity of composition, little difference in corrosion susceptibility of the two types of 316 SS tubing was observed. Therefore, for this report the data for the two will be combined and referred to as Type 316L.

Table 1.2

COMPOSITION OF SPECIMENS

Element	304	304L	316	316L
C	0.05%	0.02%	0.02%	0.02%
Mn	1.72	1.11	1.72	1.67
P	0.025	0.014	0.022	0.025
S	0.013	0.013	0.021	0.012
Si	0.32	0.66	0.47	0.54
Ni	9.25	9.93	13.49	13.10
Cr	18.75	18.65	17.95	17.87
Mo	--	--	2.10	2.78
Hardness	RB-72	RB-79	RB-77	RB-83

Immediately prior to insertion in the test loop, each specimen was cleaned and pickled in 12 v/o HNO_3 - 2 v/o HF.

At the conclusion of the test, the specimens were inspected, weighed, descaled, re-weighed, and examined. A salt-bath descaling procedure was found to be the best method for removing corrosion-product film; it was not entirely satisfactory, however, in that a blank correction of 10 mg dm^2 was required.

Test Results

Superheated steam exposure produced a uniform surface film of corrosion product. No evidence of local corrosion attack was observed.

The specimens exposed to the saturated steam (particularly that with lower quality) had a dark, blotchy appearance. These dark areas were associated with intergranular attack. Figure 1.3 shows a specimen of this type. The blotchy pattern was apparent when the specimens were removed from the test loop but did not show up well in photographs until after descaling.

Figures 1.4 and 1.5 show the surface appearance of the 316L and 304 specimens after pickling and before insertion in the loop for the test. When the specimens were removed following exposure, intergranular attack was observed in local areas. The attack increased with time of exposure, and was greatest for the Type 304. Penetration increased with moisture content of the steam. Figures 1.6, 1.7 and 1.8 indicate the type and extent of penetration found at the end of the test for those specimens exposed to the highest moisture (0.5 per cent).

The effect of moisture content and alloy composition on corrosion is further demonstrated in Table 1.3 which presents the observed weight loss (descaled) of the specimens.

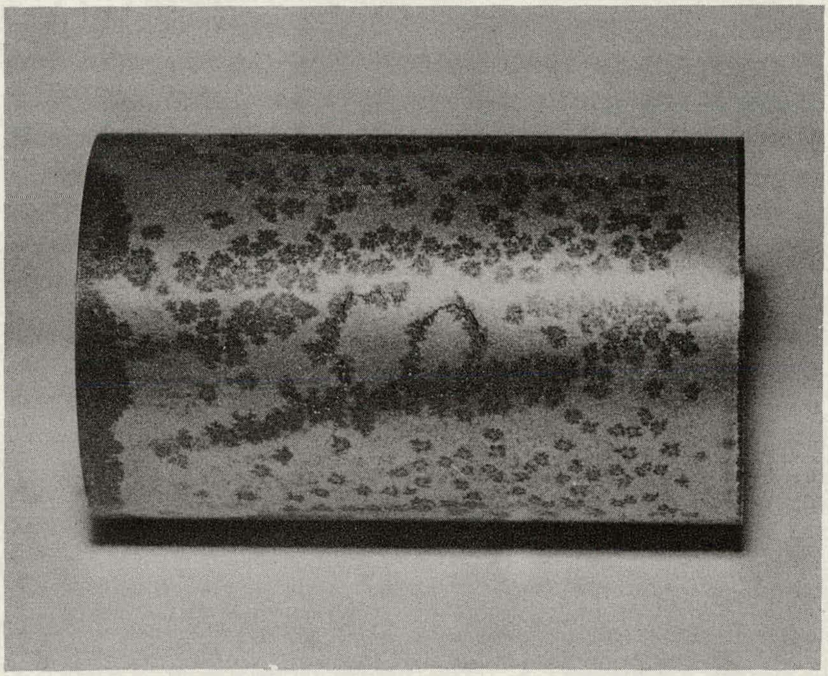

Fig. 1.3...Type 304 s/s after 15 weeks exposure to saturated steam containing 0.5 per cent moisture and 30 ppm oxygen (descaled) (108C-2)

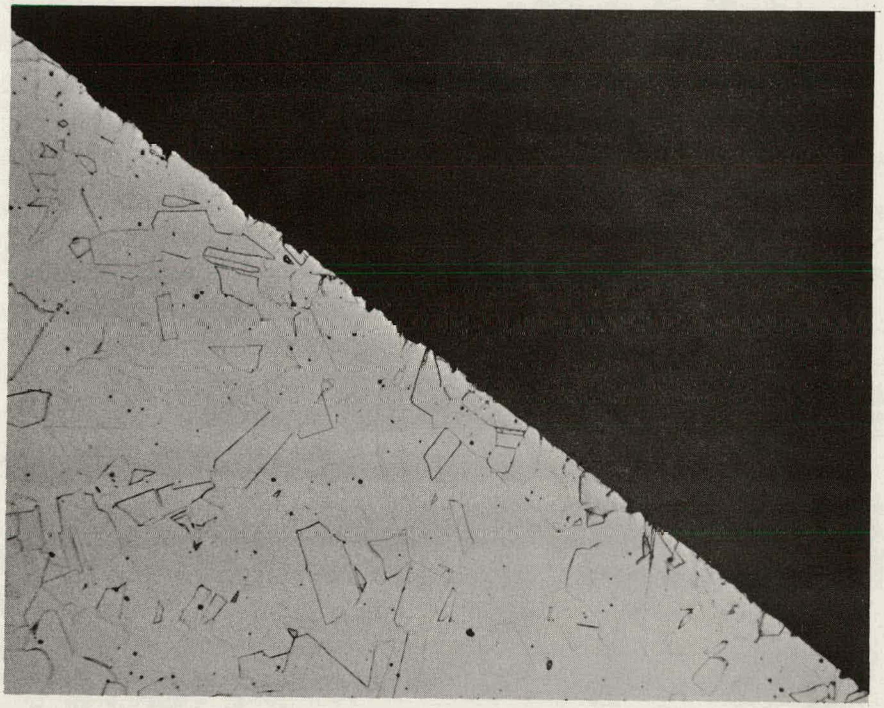

Fig. 1.4...Original pickled surface of Type 316L prior to start of testing...250X (9D-5-1)

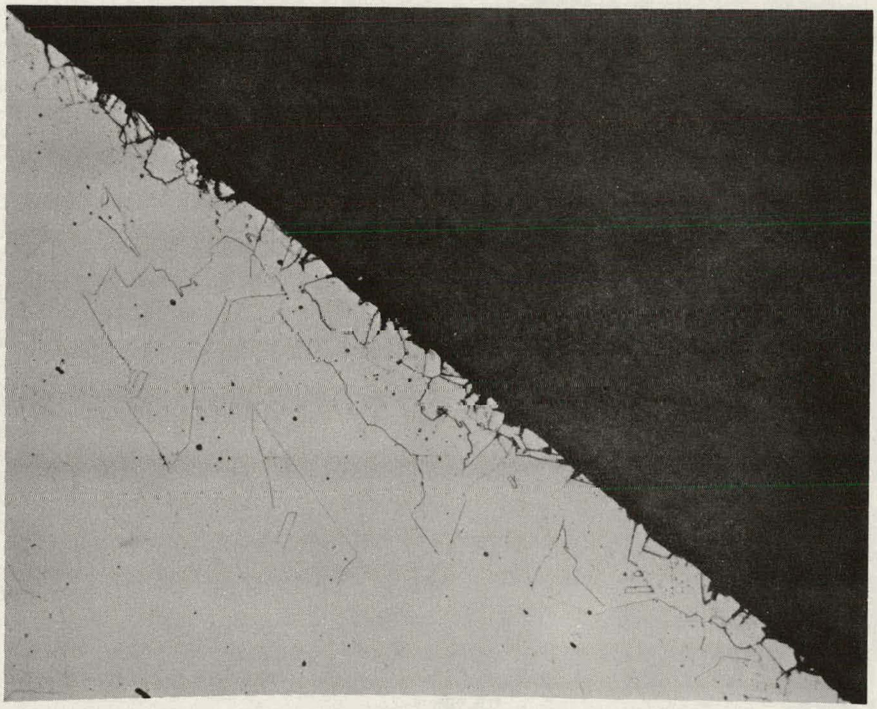

Fig. 1.5...Original pickled surface of Type 304 prior to start of testing...250X (9D-2-1)

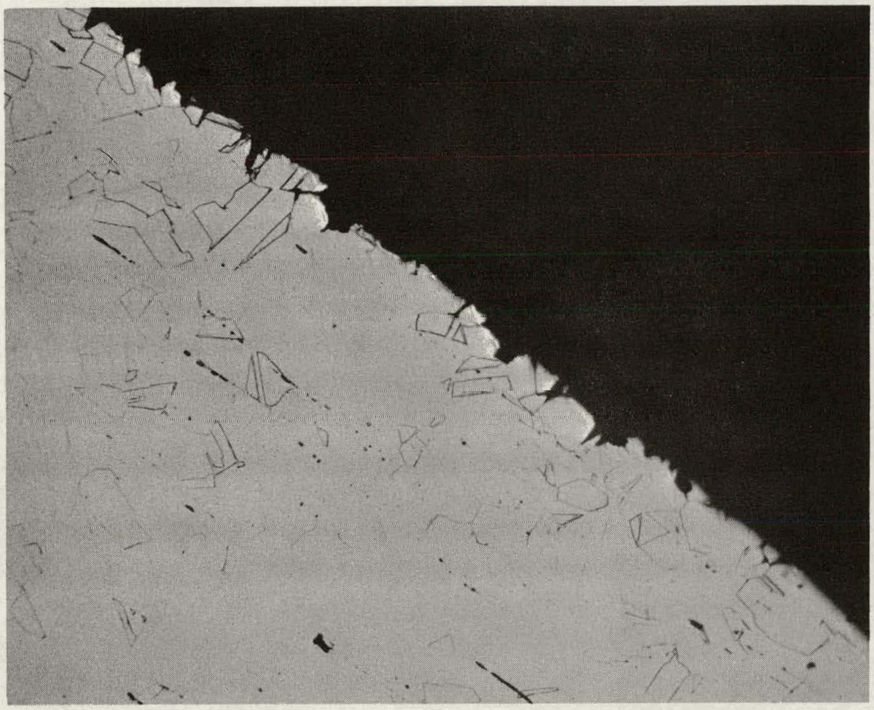

Fig. 1.6...Intergranular corrosion of Type 316L stainless steel exposed for 2500 hours to saturated steam containing 0.5 per cent moisture and 30 ppm oxygen...250X (9D-13-1)

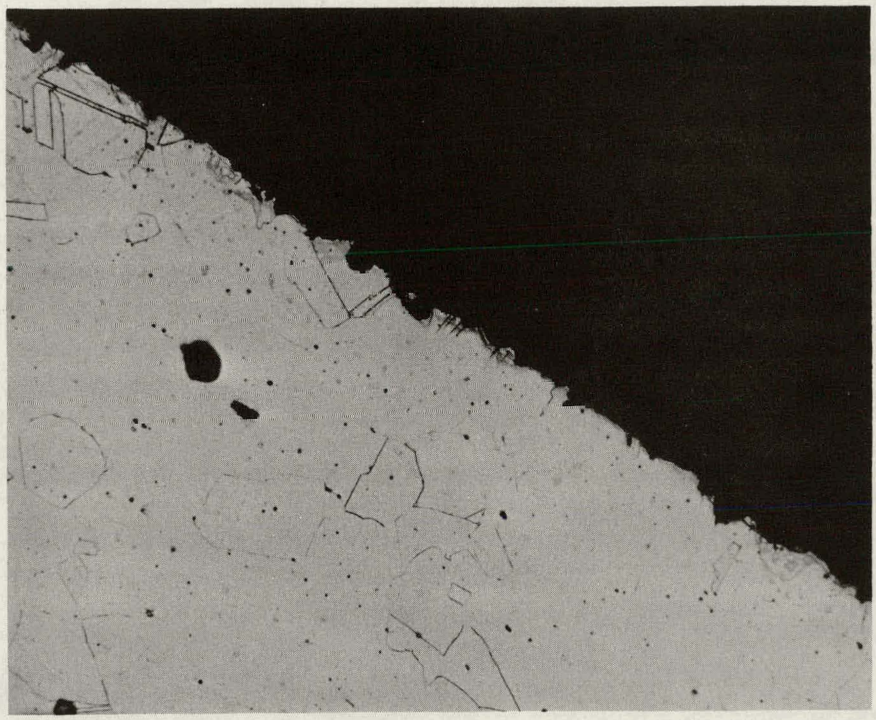

Fig. 1.7...Intergranular corrosion of Type 304L stainless steel exposed for 2500 hours to saturated steam containing 0.5 per cent moisture and 30 ppm oxygen...250X (9D-12-1)

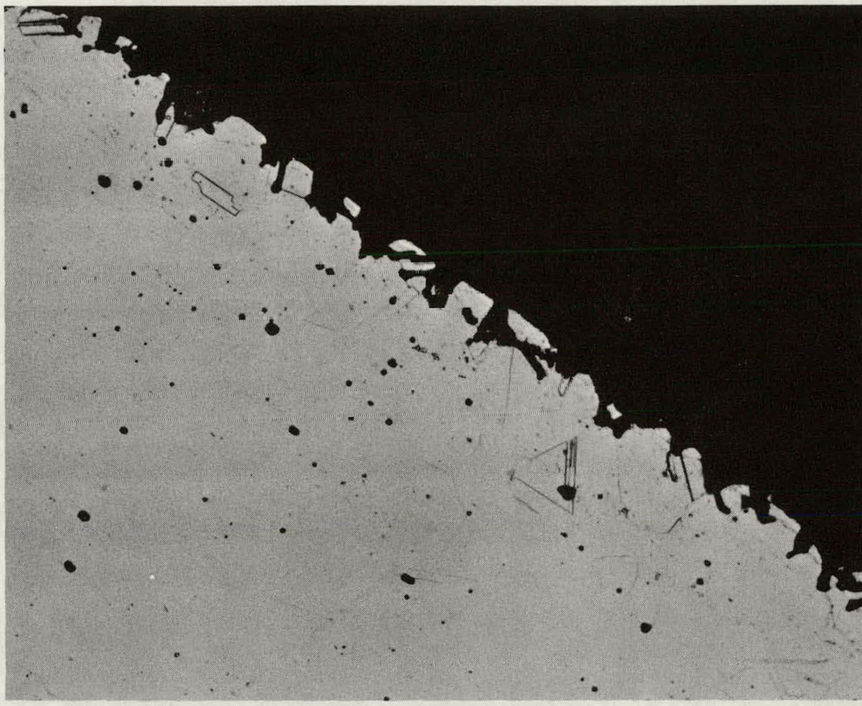

Fig. 1.8...Intergranular corrosion of Type 304 stainless steel exposed for 2500 hours to saturated steam containing 0.5 per cent moisture and 30 ppm oxygen...250X (9D-11-1)

TABLE 1.3

CORROSION IN DYNAMIC STEAM

Exposure Hours	Superheated Steam	Saturated Steam Moisture Content 0.0%	0.1%	0.5%
Type 316L				
500	15.4**	23.5*	30.3*	20.5*
1000	13.8*	14.0	31.2	37.6
1500	17.1**	19.3*	45.6*	72.4*
2000	12.8*	---	34.2	100.6
2500	7.6*	18.1*	26.9*	70.2*
Type 304L				
500	21.2*	27.6	53.4	---
1000	28.3	26.8	38.2	34.6
1500	25.6*	42.1	26.6	36.9
Type 304				
500	60.7*	53.3	58.6	61.7
1000	---	---	---	---
1500	90.3*	77.1	80.5	270.0
2000	90.7	53.1	106.8	281.4
2500	27.0	55.3	67.4	141.2

* Avg. of 2 specimens
** Avg. of 4 specimens

No explanation for the consistent decreased corrosion of the 2500-hour samples has been found.

The amount of erosion was calculated by comparison of corrosion product theoretically formed with that actually adhering to the specimen, which was removed by descaling. The amount of corrosion product formed was calculated by assuming all metal was converted to magnetite (72 w/o metal). Table 1.4 shows results of calculations on corrosion product eroded and released from the specimens. As noted for the corrosion data, release rate at 2500 hours is inconsistent with rest of data...and no explanation has been found.

Table 1.4

RELEASE OF CORROSION PRODUCT
in mg/dm^2

Exposure Hours	Superheated Steam	Saturated Steam Moisture Content 0.0%	0.1%	0.5%
Type 316L				
500	0.7**	1.8*	1.0*	-1.9*
1000	-0.8*	-4.3	-0.9	3.0
1500	1.0**	0.1*	0.0*	3.2*
2000	0.1*	-2.5	-4.1	-1.1
2500	-0.1**	-1.2*	-5.9*	0.9*
Type 304L				
500	0.0*	6.6	8.9	---
1000	5.0	2.0	4.6	5.8
1500	-0.7*	5.5	0.6	7.3
2000	---	---	---	---
2500	-4.6*	-6.1	---	---
Type 304				
500	37.6*	12.5	20.8	15.8
1000	---	---	---	---
1500	70.8*	23.0	29.8	29.4
2000	69.3	20.6	28.4	33.2
2500	5.7*	16.1	4.9	12.7

* Avg. of 2 specimens
** Avg. of 4 specimens

Summary

There is no clear differentiation among the low carbon alloys in any of the environments used in this test, either in corrosion or corrosion product release (erosion). All alloys suffered some intergranular attack in wet, oxygenated steam. The intergranular attack increased in severity with moisture content of the steam and was markedly greater for the higher carbon Type 304 stainless steel. Weight changes (descaled) verify the increased severity of corrosion with moisture quality and with carbon content of the Type 304 stainless steel alloy.

The hypothesis of no erosion of corrosion product from the Type 316L stainless steel is consistent with the experimental errors of the test. Type 304 alloy exhibited increasing release of corrosion product with carbon content and with moisture content of the steam.

1.6 DEVELOPMENT OF LOW-ENRICHMENT SUPERHEATER FUEL ELEMENTS

The objectives of this project are to determine the economic merit of using low-enrichment superheater fuel, to determine and select a promising fuel element design, and to develop a low-enrichment superheater fuel element through applicable studies, fabrication experiments, and testing.

At such a time as a promising fuel element concept has been selected, a full-scale mock-up will be fabricated including supports and steam entry and exit section, and flow tests will be performed to determine pressure drop and dimensional stability at simulated reactor operating conditions.

Heat transfer calculations will be performed. A test element will be fabricated for insertion in the heat transfer loop to perform heat transfer experiments under simulated Pathfinder operating conditions. Physics calculations will be performed, such as the required computer programming and operation, determination of the critical mass, neutron and gamma flux and power distribution, enrichment, coefficients of reactivity, control rod effectiveness, and conversion ratio.

A partial loading of prototype low-enrichment elements will be fabricated and tested in the critical facility in conjunction with the remainder of the superheater section of the core containing high-enrichment fuel elements. Safeguards reports will be prepared for the facility as required to meet the licensing requirements of the AEC. Critical experiments will be conducted to determine the nuclear characteristics of the prototype low-enrichment superheater fuel elements.

1.6.1 NUCLEAR DESIGN

1.6.1.1 Development of Low-Enrichment Superheater Analytical Model

Calculated Thermal Multiplication Factors

The development of an analytical model for determining clustered pin superheater lattice thermal utilization has been completed. The final step in this development entailed adapting the physical and mathematical treatment contained in the Philco-2000 MARC code to the superheater cell.

MARC is a thermal multigroup, XY geometry transport program using the Monte Carlo mathematical approach. Except for the multigroup feature, MARC is similar to the TRAC-I code described in ACNP-62034 (Pathfinder July-September 1962 Quarterly). For the MARC calculations, a cross section library was constructed using a 23 C Nelkin kernel, hydrogen energy transfer cross sections[1], hydrogen average scattering cosine values determined by the Radkowsky prescription (as in SOFOCATE), and microscopic absorption and fission cross sections from BNL-325, 2nd edition.

Results

Normalized regionwise fission response levels obtained from MARC are given in Table I.5. The experimental values, and those from previously attempted (and reported) analytical methods are repeated to make the tabulation complete.

Ref. I. Kerr, B. "Calculated Scattering Kernels for Light Water", GEAP-3944, May, 1962.

TABLE 1.5

THERMAL FLUX WEIGHTING FACTORS

METHOD	REGION				
	Center Pin	Outer Pin	Wall	Moderator	
	Voided, 7 pin, 3-1/2 w/o, Single-Walled B Cell				
Experiment	.756 ± .008	.821 ± .003	1.091 ± .010	1.210 ± .001	
I_2 - SOFOCATE	.810	.894	1.032	1.127	
TRAC-SOFOCATE	.769 ± .024	.817 ± .017	1.037 ± .021	1.147 ± .026	
MARC	.727 ± .024	.799 ± .014	1.037 ± .017	1.205 ± .017	
	Voided, 7 pin, 3-1/2 w/o, Single-Walled D Cell				
Experiment	.794 ± .007	.850 ± .003	1.085 ± .009	1.198 ± .011	
I_2 - SOFOCATE	.862	.935	1.019	1.123	
TRAC-SOFOCATE	.826 ± .029	.840 ± .015	1.013 ± .021	1.139 ± .020	
MARC	.821 ± .022	.829 ± .017	1.013 ± .020	1.211 ± .026	
	Voided, 7 pin, 3-1/2 w/o, Double-Walled B Cell				
Experiment	.738 ± .008	.799 ± .003	1.025 ± .010	1.211 ± .010	
I_2 - SOFOCATE	.802	.884	1.015	1.142	
TRAC-SOFOCATE	.777 ± .020	.825 ± .010	.983 ± .016	1.160 ± .015	
MARC	.724 ± .02	.793 ± .013	.983 ± .017	1.238 ± .021	
	Voided, 7 pin 7 w/o, Double-Walled B Cell				
Experiment	.617 ± .005	.710 ± .002	1.061 ± .009	1.309 ± .010	
I_2 - SOFOCATE	.669	.807	1.038	1.215	
TRAC-SOFOCATE	.634 ± .034	.731 ± .012	1.005 ± .019	1.216 ± .020	
MARC	.576 ± .020	.693 ± .014	1.005 ± .016	1.325 ± .023	
	Flooded, 7 pin, 3-1/2 w/o, Single-Walled B Cell				
	Center Pin	Outer Pin	Wall	Moderator	Flooding Water
Experiment	.677 ± .005	.770 ± .002	1.128 ± .007	1.185 ± .008	.966 ± .006
I_2 - SOFOCATE	.714	.796	1.091	1.129	.978
TRAC-SOFOCATE	.694 ± .016	.794 ± .017	1.103 ± .026	1.158 ± .021	.975 ± .022
MARC	.642 ± .025	.732 ± .022	1.134 ± .033	1.187 ± .035	.979 ± .021

The cases previously indicated include all MARC calculations. Experimental and MARC values are U-235 fission activities...the I_2 and TRAC values are thermal fluxes. The experimental uncertainties reflect counting statistics only. The Monte Carlo MARC and TRAC uncertainties correspond to the 95 per cent confidence level. They arise, in a formal mathematical fashion, from the variation inherent in making statistical estimates.

Disagreement between analyses and experiment for the wall flux level is not serious. No direct measurements in the wall were made; the "measured" wall flux was therefore defined in a somewhat arbitrary way.

Thermal multiplication factors (Nf_2) are given in Table I.6. These integrated quantities are not regarded as sensitive criteria for comparing analysis and experiment.

TABLE I.6

THERMAL MULTIPLICATION

Case	Method			
	Experiment	I_2	TRAC	MARC
Voided 7 pin 3-1/2 w/o Single Walled B cell	1.355	1.394	1.362 ± .015	1.355 ± .025
Voided 3-1/2 w/o Single Walled D cell	1.361	1.405	1.372 ± .011	1.355 ± .025
Voided 3-1/2 w/o Double walled B cell	1.202	1.247	1.226 ± .010	1.208 ± .020
Voided 7 w/o Double Walled B cell	1.474	1.522	1.504 ± .016	1.468 ± .029
Flooded 3-1/2 w/o Single Walled B cell	1.226	1.249	1.238 ± .019	1.222 ± .039

Superheater Design Summary

It is now feasible to attempt clustered pin superheater designs. The MARC code would be necessary to obtain reference results and to verify the final cell configuration. Utilizing Monte Carlo analyses requires designing toward an acceptable range of superheater performance. For example, the MARC computed Nf_2 values imply a reactivity uncertainty of about 3-1/2 per cent, which corresponds to an outlet steam temperature uncertainty of about 80 F. However, it is practical to increase the Monte Carlo sample size (and calculational expense) enough to reduce this to a 40 F. band.

Other uncertainties are additional. Important ones are those involved in computing resonance absorption and those associated with the basic cross section data. The Hellstrand formula has been found to be the most reliable technique for calculating resonance integrals for these clustered-pin cells. However, the adaption of Hellstrand's UO_2 formula to a situation differing from that in which Hellstrand's experiments were performed introduces uncertainty into the low enriched superheater design. Therefore, the uncertainty associated with the Hellstrand formula should be regarded as a lower limit on total uncertainty for superheater design.

3. NUCLEAR ANALYSIS

3.1 REACTOR PHYSICS (STATICS)

The objective of this project is to perform physics calculations such as computer programming and operation, and to determine the critical mass, neutron and gamma flux and power distribution, enrichment, coefficients of reactivity, control rod effectiveness, and conversion ratio with respect to a Pathfinder core with an integral high-enrichment superheater region. An additional objective is to determine shielding requirements for the Pathfinder Plant.

3.1.1 PATHFINDER FIRST CORE BORON STAINLESS STEEL POISON SHIMS

To allow for more reactivity control for the first Pathfinder core, boron stainless steel strips will be available for insertion between the fuel assemblies of the boiler core. The shims are 0.1 inch thick, contain 0.2 w/o natural boron, and are the same length as the active fuel assembly. Each of the thirty-two non-quad box fuel assemblies has been fabricated with slots on the outside into which these boron strips fit. Figures 3.1 and 3.2 show the available core locations for these strips and a cross section of the modified fuel assembly and boron strip respectively.

To insure maximum shutdown margin during Phase I of the reactor startup program, a number of the shims will be loaded into the core initially and removed as part of the test program. If it becomes necessary to leave some in the core during reactor operation to meet the one-control-rod-stuck criteria or for other reasons, selected core locations would be utilized which yield the maximum reactivity control cold, but result in a minimum reactivity loss to the hot operating reactor. A nuclear analysis to determine these locations and the absolute reactivity worth of the shims has been made and the results are

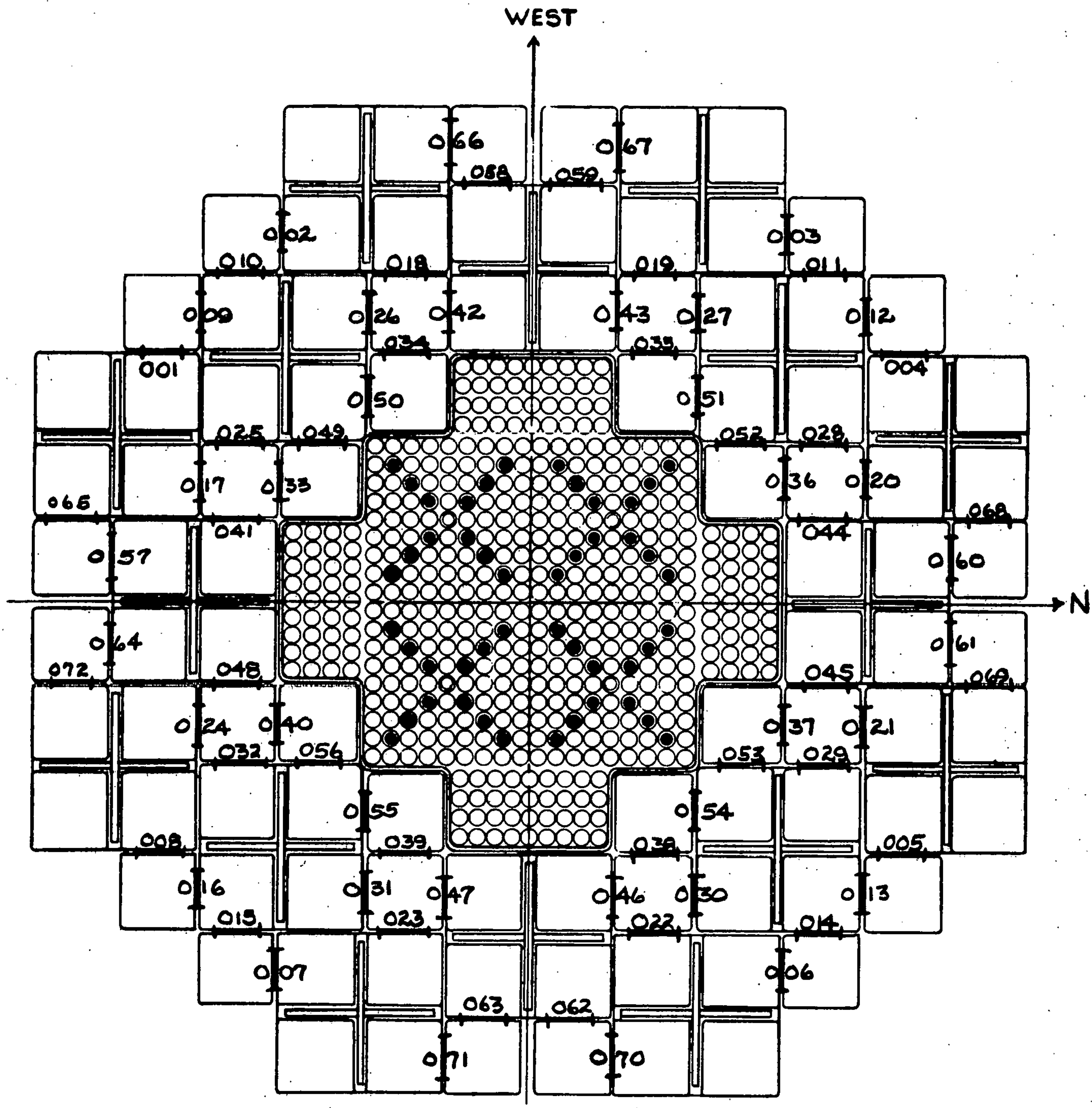

Fig. 3.1...Boron-Stainless Steel Shim Locations

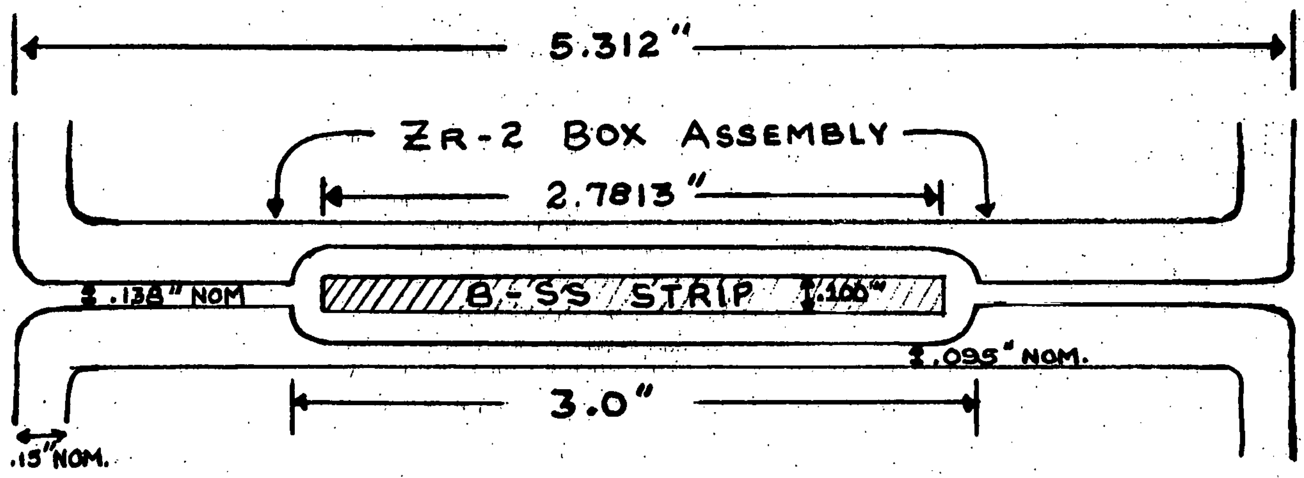

BORON-STAINLESS STEEL STRIP .2 w/o NAT. BORON

Fig. 3.2...Modified Fuel Assembly and Boron-Stainless Steel Strip

contained in this quarterly report.

The objectives of this analysis were as follows:

1. determine the absolute reactivity worth of all the shims for the cold, all-control-rods-inserted core;
2. determine the relative worth of the various locations in which the shims can be inserted for the cold, rodded core;
3. determine the absolute worth of shims in selected locations for the cold core with the maximum-worth control rod withdrawn and all other control rods inserted;
4. determine the relative worth of locations for the hot-voided, all-control-rods-withdrawn core;
5. determine the absolute worth of shims in selected locations for the hot-voided, non-rodded core; and
6. determine the effect on the flux distribution of locating shims in the hot operating reactor.

Perturbation theory was used to evaluate objectives 1, 2, 4, and 5. Two-dimensional, explicit diffusion theory calculations were used to evaluate objectives 3 and 6, and to check the adequacy of perturbation theory for the other calculations.

Two-dimensional, two-group, adjoint calculations were performed for the cold, clean, all-control-rods-inserted core and for the hot, voided, all-control-rods-withdrawn core. These, along with the flux calculations performed for the identical core configuration, were used to determine the importance function for the various shim locations. The reactivity worth of the shims was found using the following expression,

$$\Delta k/k = \frac{1}{F}\Big[-\int \phi_2^* \phi_2 \delta\Sigma_{a_2} dV + \int \phi_1^* \phi_2 \delta\nu\Sigma_{f_2} dV$$

$$+ \int \phi_1^* \phi_1 \delta\nu\Sigma_{f_1} dV - \int \phi_1^* \phi_1 \delta\Sigma_{a_1} dV + \int \phi_1 (\phi_2^* - \phi_1^*) \delta\Sigma_{R1} dV\Big]$$

$$F = \int \phi_1^* \phi_2 \, \nu\Sigma_{f2} dV + \int \phi_1^* \phi_1 \nu\Sigma_{f1} dV$$

In this expression, only changes to the thermal absorption were considered, $\delta\Sigma_{a2}$. Changes to the removal cross section, $\delta\Sigma_{R1}$, are negligible because the stainless steel strip merely replaced the metal milled from the side of the fuel assembly. Thermal self shielding was not considered for the perturbation analysis $[\Sigma_a t \text{ (2200 M/sec)} = .24]$, nor was the contribution to the fast absorption considered, $\delta\Sigma_{a1} = 0$. These are compensating effects.

Diffusion theory was used in those calculations in which the shims were explicitly represented. The capture difference between diffusion theory and transport theory, P_1 and P_3 approximation, was determined one-dimensionally and incorporated into the diffusion theory calculation by adjustment of Σ_{a2} of the strip.

Explicit two-dimensional PDQ-XY calculations were made for the cold clean core with all but the maximum-worth control rod inserted and for the hot operating core with no control rods inserted. For both problems, shims were placed in selected symmetric locations. The hot operating calculation was used to check the adequacy of the perturbation analysis as well as the effect of the shim on the core flux distribution.

Table 3.1 gives the absolute worth of individual shims in the various locations as well as the total worth of all of the shims for both the cold and hot operating conditions. These results were obtained from the perturbation analysis.

Table 3.1 - REACTIVITY WORTH OF BORON STAINLESS STEEL SHIMS

No. Shims	and Shim Location in Core*	Worth (Δk/k) Cold (All Rods In) Core	Worth (Δk/k) Hot (All Rods Out) Voided Core
8 Shims	001 thru 008	-.00315	-.00355
8 Shims	009 thru 016	-.00408	-.00364
8 Shims	017 thru 024	-.00900	-.00621
8 Shims	025 thru 032	-.01004	-.00657
8 Shims	033 thru 040	-.01250	-.00567
8 Shims	041 thru 048	-.00981	-.00573
8 Shims	049 thru 056	-.01069	-.00575
8 Shims	057 thru 064	-.00384	-.00458
8 Shims	065 thru 072	-.00242	-.00290
	72 Shims	-.0655	-.0446

*See Fig. 3.1 for positions in core.

Calculations have indicated that the worth of the maximum-worth control rod could be as much as 0.05 Δk/k. The shutdown margin for the first core reference loading (96 2.2 w/o enriched boiler elements and 50 kg U-235 in superheater elements) is calculated to be at least 0.035 Δk/k. Thus, to meet the one-rod stuck criteria, it may be necessary to add another 0.015 Δk/k in shutdown to the cold core. This could be accomplished by the selective location of sixteen shims, positions 041-056 in Figure 3.1. These locations would satisfy the following requirements: 1) provide the greatest negative reactivity addition in the cold rodded core, 2) provide the most reactivity control around the maximum worth control rod, and

3) give the smallest negative reactivity addition in the hot operating core. The eight inner control rods provide the greatest reactivity control worth and all of the above shim positions are adjacent to the fuel elements about the inner rods. The combined worth of these sixteen shims in the cold rodded core is 0.0205 $\Delta k/k$ and only 0.0115 $\Delta k/k$ in the hot, non-rodded operating core.

It was for these locations that the explicit shim insertion problems were run. The results for the hot operating core are shown in Table 3.2. Note the close agreement with results obtained from the perturbation analysis and the negligible effect on the flux distribution or power peaking.

Table 3.2 - EFFECT OF BORON STRIPS IN SELECTING LOCATIONS OF HOT OPERATING CORE

No.	Core	Reactivity Worth ($\Delta k/k$)		Peak/Ave. Power (Boiler)	
Shims	Location	Eigenvalue $\Delta\lambda$	Perturbation	Without Shims	With Shims
16	041-056	-.0119	-.0115	1.737	1.727

The absolute worth of these sixteen shims, positions 041-056 in the cold, one-control-rod-withdrawn core is shown in Table 3.3. The uncertainties in the analysis which arise from convergence and shim representation are included.

Table 3.3 - WORTH OF BORON STRIPS IN SELECTED LOCATIONS OF COLD CORE, MAXIMUM-WORTH CONTROL ROD WITHDRAWN

No. Shims	Core Location	Worth ($\Delta k/k$)
16	041-056	.020 to .026

A summary of the core shutdown requirements with and without the negative shims can be seen in Table 3.4. Also given in this table are the shutdown requirements and expected operating excess reactivity with all but sixteen of the shims removed. Both the shutdown margin and operating excess reactivity shown are for the reference core loading.

Table 3.4 - SUMMARY OF CORE SHUTDOWN REQUIREMENTS

	Cold Clean Shutdown Margin ($\Delta k/k$)	Hot Full Power Excess Reactivity ($\Delta k/k$)
1. Reference Core Loading - No Shims	-.035	.021
2. Reference Core Loading - All Shims	-.100	
3. Reference Core Loading - 16 Shims (041-056 added)	-.055	.010

If poison shims are required to meet the one-rod-out criterion, they would be removed after several months of power operation.

3.2 REACTOR AND SYSTEM DYNAMIC ANALYSIS

The objectives of this project are to perform reactor transient analyses under normal operation and after credible or hypothetical accidents involving equipment failure or reactor misoperation, as well as a system stability analysis using an analog simulator or digital computer.

3.2.1 PATHFINDER TRANSIENT SIMULATOR

Investigations on the Pathfinder simulator of runback and changing recirculation flow rate confirmed results previously reported (ACNP-62035, Pathfinder Technical Progress Report, October-December, 1962). Also studied was the withdrawal of a control rod with time variable flux peaking. This experiment was performed to determine whether a time-dependent peaking factor affected previously reported transient results. Analysis of the experiments is continuing.

Additional transfer function measurements were taken on the Pathfinder simulator for several different power-to-recirculation flow ratios. These results showed that the Pathfinder closed loop transfer function, at various power-to-flow ratios, will have shapes similar to the rated full-power condition. Complete reports of these calculations will be presented in the technical report "Pathfinder Simulator Results" which is presently being written.

Further analysis was made on a two-region reactor model to determine spatial effects of the boiler and superheater regions during system transients. This work is continuing.

PART B

POST CONSTRUCTION R&D

1.0 INITIAL STABILITY AND PERFORMANCE TESTS

The objectives of this project are to design and fabricate a special oscillator rod and drive mechanism together with suitable instrumentation and recording equipment to measure and record the resulting variations in neutron flux, and to conduct oscillator tests to verify dynamic performance calculations and to determine experimentally the stability of the reactor system.

1.0.1 OSCILLATOR ROD BUSHINGS

An individual test was run to determine if the 17-4 PH chrome-plated bushings for the 17-4 PH drive shafts were satisfactory for operation of the bushing and shafts in 489 F steam. Test setup used for this test was the same as used for testing bearings for the Pathfinder oscillator rod.

The test was run for 305 hours. Test conditions were as follows: a low pressure 489 F steam environment...no external radial or thrust loading...350 rpm shaft speed.

Upon completion of the test, inspection revealed that black streaks had formed on both the chromeplated bushing surface and the shaft surface, but there was no evidence of galling. The ID of the bushing and the OD of the shaft were measured. This showed that there was very little wear on either surface; hence, the bushing design was considered satisfactory.

1.0.2 OSCILLATOR ROD ASSEMBLY

The Pathfinder oscillator rod assembly was completed during this Quarter and the control cabinet was assembled and tested.

A test was run on the oscillator rod assembly to determine if the assembly would function properly, and also to check if all components would meet performance specifications.

The test was run in cold, demineralized water in a 40-ft deep tank. The test setup, as originally assembled in air, is illustrated in Figures 1.01, 1.02, and 1.03. The setup outside of the tank was made in order to set the sine-cosine potentiometer to give a signal which would be in phase with the actual reactor input signal. To do this, the motor was run very slowly until the cadmium on the rotor and on the stator of the oscillator were directly in line. Then the motor was shut off and the potentiometer was set to give its maximum voltage output.

The test setup was disassembled and reassembled in the tank which was filled with demineralized water. The tower was not mounted on the drive assembly but was submerged in the tank with the tubing assembled on the tower. The test was run for a total of 25 hours, including operation of the motor at 350 rpm for 20 hours. During the remaining time, the motor was run at various speeds.

The following observations were made during the test: The bearing supports did not reach their natural frequency at maximum speed (350 rpm) and their design, therefore, is satisfactory. Motor current increased for a fixed speed as the test progressed...due to leakage of the motor housing oil into the transmission, which caused an overloading condition. The breaker points, set with a .005-in. gap, did not arc in the oil; they functioned perfectly.

Upon completion of the test, the test setup was dismantled and the internals of the oscillator rod assembly were taken apart for checking. Results of the inspection showed:

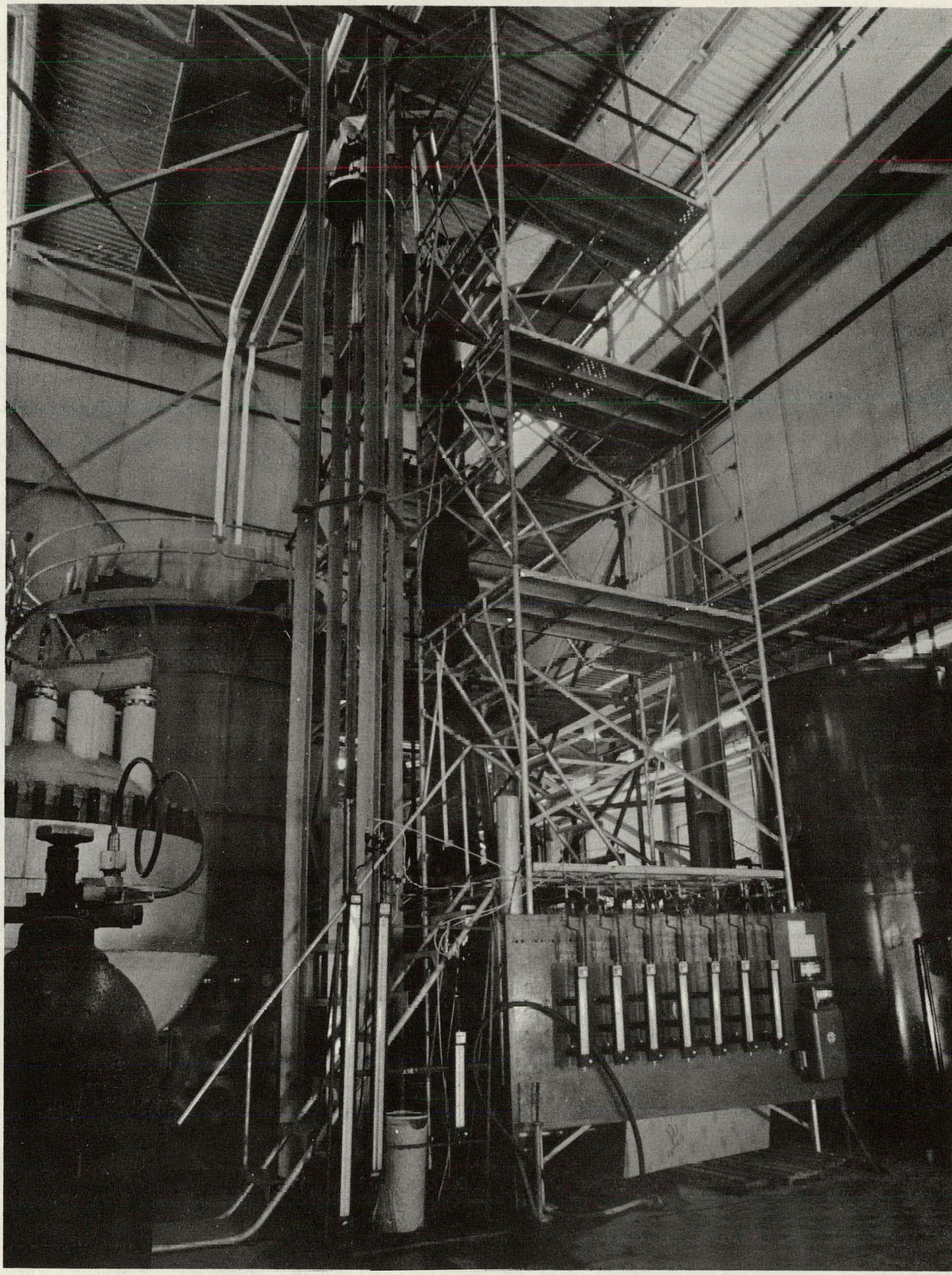

Fig. 1.01...Oscillator Rod on Test Assembly (7D-0-1)

Fig. 1.02...Oscillator Rod Internals on Test Assembly (7D-0-2)

Fig. 1.03...Oscillator Rod Drive Unit on Test Assembly (7D-0-3)

There was no measurable wear on any of the graphite bearing surfaces and there was no evidence of pitting of the graphite bearing or chromeplated bearing surfaces.

The chromeplated bushing and the 17-4 PH drive shaft were inspected. No galling was found on either bearing surface.

The connection between the lower and upper drive shafts was checked. The lead-in surface of the connection (which is pinned to the lower drive shaft) showed several scratches. This, however, was anticipated since the key on the upper drive shaft had a heavy chromeplate which was much harder than the material from which the connection was made. Other than this, the connection and the key showed no sign of wear or damage.

The rotor and the stator showed no evidence of rubbing and the stator showed no indication of being overstressed while handling the internals assembly.

The breaker points, gapped at .005 in., did not pit.

The Amphenol submersion-proof connectors did not leak either oil or water.

Close inspection for corrosion was conducted on all components. It was found that rust had formed only at welds which had not been properly cleaned.

The following preventive measures were taken: the drive motor unit was returned to the manufacturer for replacement of all the gaskets (to ensure proper sealing of the unit)...and the welds which had rusted were cleaned to prevent any re-forming of rust.

The instrumentation system to be used in conjunction with the oscillator was completed. The system test showed several minor discrepancies in the instrumentation system. These were corrected, however, and the system now operates in a satisfactory manner. Figure 1.04 is an illustration of the completed pile oscillator instrumentation system. The components, from top to bottom, are: a) Computer patchup problem board and potentiometer strip...b) Computer...c) Digital voltmeter... d) Micromicroammeter...e) Strip chart recorder...f) Recorder amplifier... g) Oscillator and instrumentation operating console...h) Electronic multiplier...i) Fan unit. Figure 1.05 is a circuit block diagram of the instrumentation system. Figure 1.06 is a closeup of the operating console. The entire oscillator mechanism and instrumentation system will be operated from this console. The instrument cabinet will be located in the control room.

The computer section of the oscillator instrumentation system will be used, in the near future, to take a trial run transfer function of the Pathfinder transient simulator.

Conclusions reached from these tests are that the oscillator rod assembly will perform satisfactorily when assembled in the Pathfinder reactor, and that all materials are compatible and meet design specifications.

1.0.3 IN-CORE ION CHAMBERS

The in-core ion chamber instrumentation is being assembled into a system. This project is expected to be completed during the next quarterly period.

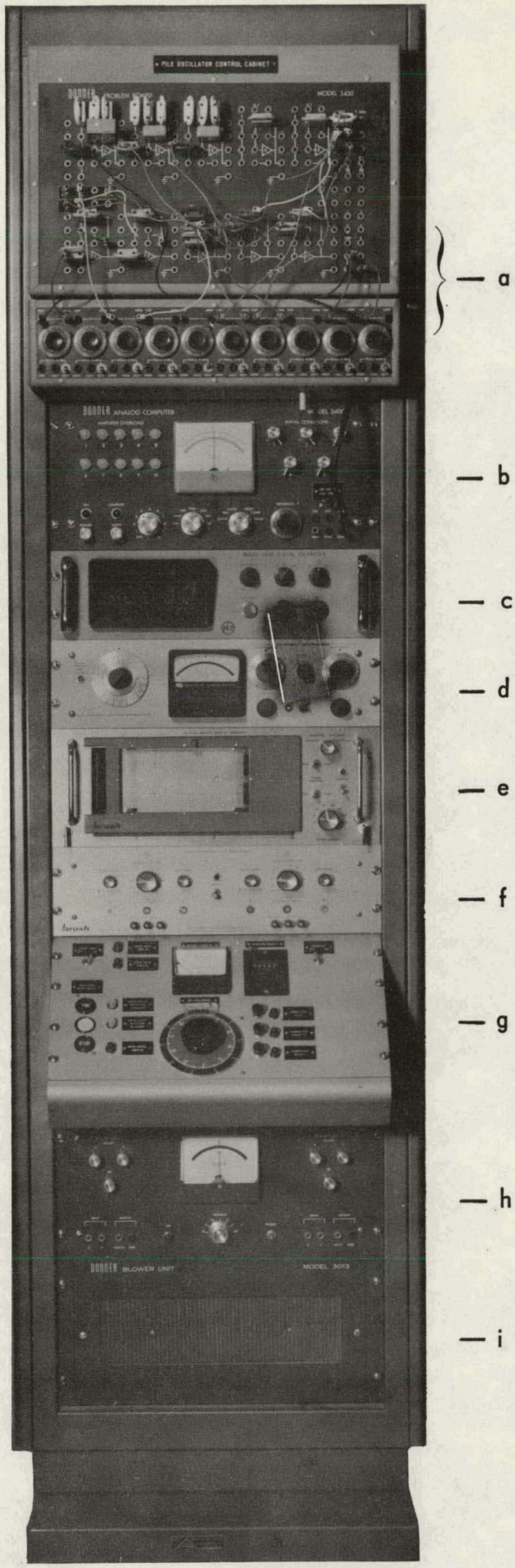

Fig. 1.04...Completed Instrumentation System (28D-0-4)

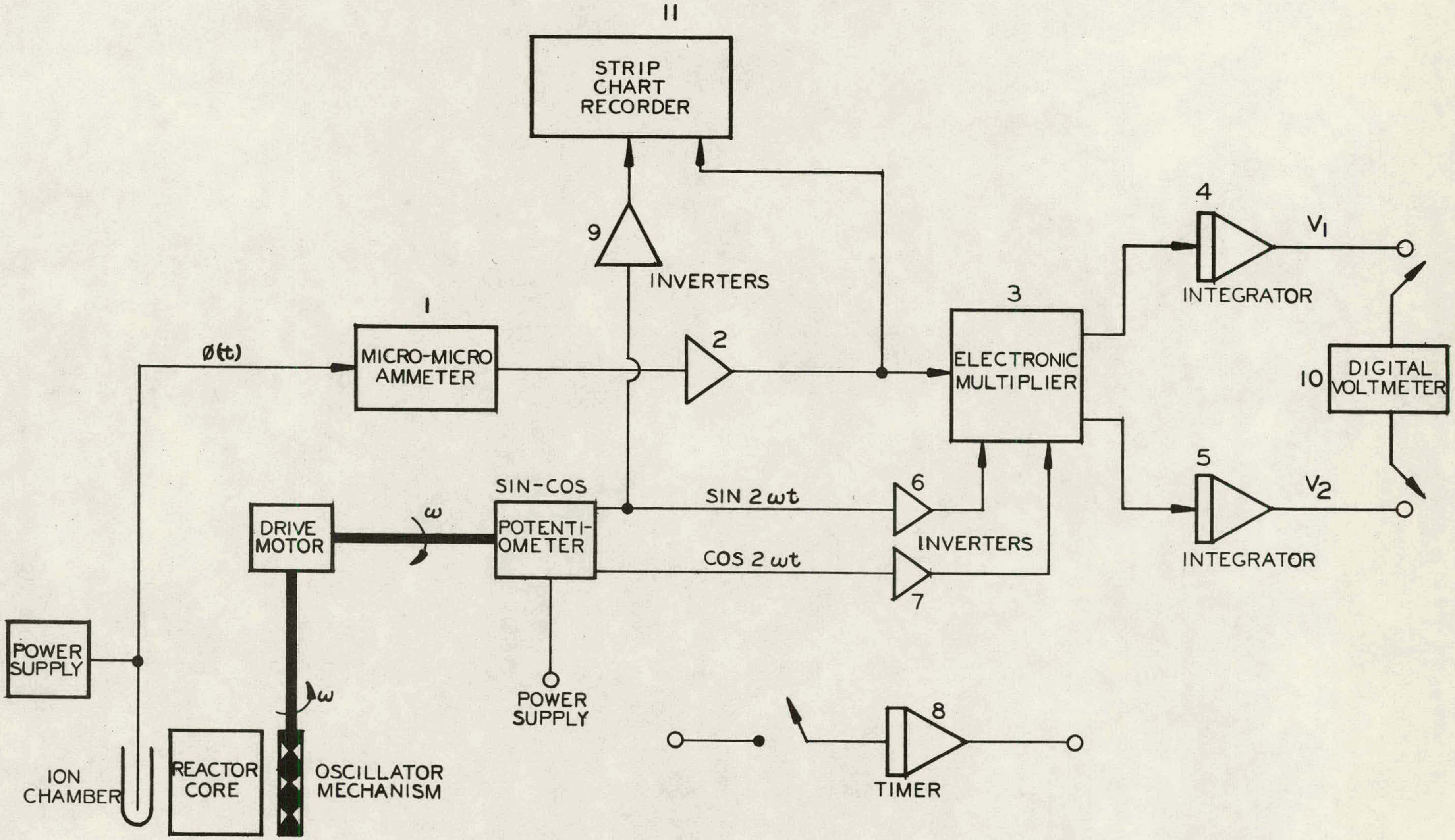

Fig. 1.05...Pathfinder Pile Oscillator Instrumentation Schematic Diagram (43-025-297)

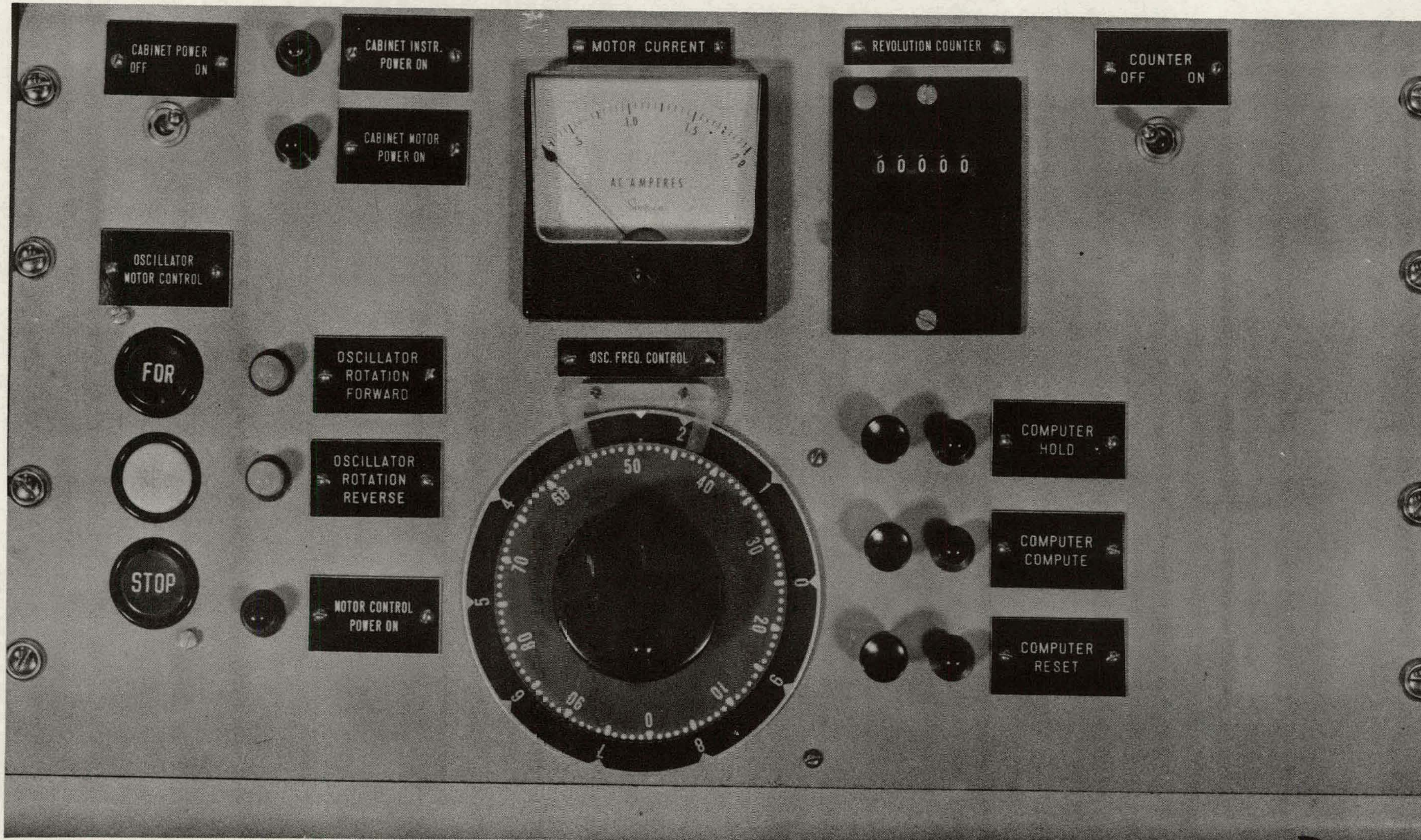

Fig. 1.06...Closeup of Operating Console (28D-0-6)